

**Dieses Dokument ist eine Zweitveröffentlichung (Postprint) /**

**This is a self-archiving document (accepted version):**

Sohaib Abdal, Imran Siddique, Ali Ahmadian, Soheil Salahshour, Mehdi Salimi

**Enhanced heat transportation for bioconvective motion of  
Maxwell nanofluids over a stretching sheet with  
Cattaneo–Christov flux**

Erstveröffentlichung in / First published in:



*Mechanics of Time-Dependent Materials*. 2022. Springer Link. ISSN 1573-2738.

DOI: <https://doi.org/10.1007/s11043-022-09551-2>

Diese Version ist verfügbar / This version is available on:

<https://nbn-resolving.org/urn:nbn:de:bsz:14-qucosa2-843458>

# Enhanced heat transportation for bioconvective motion of Maxwell nanofluids over a stretching sheet with Cattaneo–Christov flux

Sohaib Abdal<sup>1</sup> · Imran Siddique<sup>2</sup> · Ali Ahmadian<sup>3,4</sup>  · Soheil Salahshour<sup>5</sup> · Mehdi Salimi<sup>6,7</sup> 

## Abstract

The main aim of this work is to study the thermal conductivity of base fluid with mild inclusion of nanoparticles. We perform numerical study for transportation of Maxwell nanofluids with activation energy and Cattaneo–Christov flux over an extending sheet along with mass transpiration. Further, bioconvection of microorganisms may support avoiding the possible settling of nanoentities. We formulate the theoretical study as a nonlinear coupled boundary value problem involving partial derivatives. Then ordinary differential equations are obtained from the leading partial differential equations with the help of appropriate similarity transformations. We obtain numerical results by using the Runge–Kutta fourth-order method with shooting technique. The effects of various physical parameters such as mixed convection, buoyancy ratio, Raleigh number, Lewis number, Prandtl number, magnetic parameter, mass transpiration on bulk flow, temperature, concentration, and distributions of microorganisms are presented in graphical form. Also, the skin friction coefficient, Nusselt number, Sherwood number, and motile density number are calculated and presented in the form of tables. The validation of numerical procedure is confirmed through its comparison with the existing results. The computation is carried out for suitable inputs of the controlling parameters.

✉ A. Ahmadian  
[ahmadian.hosseini@unirc.it](mailto:ahmadian.hosseini@unirc.it)

✉ M. Salimi  
[msalimi@stfx.ca](mailto:msalimi@stfx.ca)

<sup>1</sup> School of Mathematics, Northwest University, No.229 North Taibai Avenue, Xi'an 7100069, China

<sup>2</sup> Department of Mathematics, University of Management and Technology, Lahore, Pakistan

<sup>3</sup> Decision Lab, Mediterranean University of Reggio Calabria, 89124 Reggio Calabria, Italy

<sup>4</sup> Department of Mathematics, Near East University, Nicosia, Turkey

<sup>5</sup> Faculty of Engineering and Natural Sciences, Bahcesehir University, Istanbul, Turkey

<sup>6</sup> Department of Mathematics, Statistics, and Computer Science, St. Francis Xavier University, Antigonish, Canada

<sup>7</sup> Center for Dynamics, Faculty of Mathematics, Technische Universität Dresden, 01062, Dresden, Germany

**Keywords** Maxwell nanofluid · Mass transpiration · Magnetohydrodynamics · Bioconvection · Extending sheet · Runge–Kutta scheme

## Nomenclature

### *Latin symbols*

$u_1, u_2$	velocity components (m/s)
$x, y$	Cartesian coordinates (m)
$U_w$	stretching velocity of plate (m/s)
$B_0$	magnetic field strength (T)
$C$	concentration of nanoparticles
$T$	temperature of nanoparticles (K)
$N$	Microorganism distribution
$g$	gravity ( $\text{m/s}^2$ )
$k_1$	vortex viscosity
$\rho_p$	liquid density
$C_p$	volume friction constant
$\rho_m$	motile microorganism density
$D_B$	Brownian motion coefficient ( $\text{m}^2/\text{s}$ )
$D_T$	thermophoresis constant ( $\text{m}^2/\text{s}$ )
$D_n$	diffusion constant of microorganisms ( $\text{m}^2/\text{s}$ )
$T_\infty$	ambient temperature (K)
$C_\infty$	ambient concentration of nanoparticles
$N_\infty$	ambient motile microorganisms
$\tau_1$	relaxation time of heat flux
$m$	fitted rate parameter
$E_a$	activation energy (J/mol)
$b_1$	chemotaxis constant (m)
$b$	thermal relaxation constant
$W_c$	maximum swimming cell speed (m/s)
$n$	rotation of microorganisms (1/s)
$q_w$	heat transfer rate ( $\text{W/m}^2$ )
$M$	magnetic parameter
$K_p$	porosity parameter
$Nr$	buoyancy ratio parameter
$Rb$	Rayleigh number
$Pr$	Prandtl number
$Nbt$	diffusivity ratio
$Nc$	ratio of heat capacities
$Le$	Lewis number
$Sc$	Schmidt number
$E$	activation energy coefficient
$Lb$	bioconvection Lewis number
$Pe$	Peclet number
$H$	suction/injection parameter
$A$	chemical reaction rate

### *Greek symbols*

$\alpha$	thermal diffusivity ( $\text{m}^2/\text{s}$ )
----------	---

$\beta$	Deborah number
$v_{nf}$	kinematic viscosity ( $m^2/s$ )
$\lambda$	fluid relaxation time
$\sigma$	electrical conductivity (S/m)
$\rho$	density ( $kg/m^3$ )
$\gamma$	average volume of microorganisms
$\omega$	mixed convection
$\eta$	similarity variable
$\theta$	similarity temperature
$\phi$	similarity concentration of nanoparticles
$\chi$	similarity density of micro-organisms
$\delta$	temperature difference
$\Omega$	microorganism concentration difference

### *Subscripts*

$p$	nanoparticles
$w$	on the sheet surface
$\infty$	Ambient

## 1 Introduction

Mostly, bacteria show the pattern of flow such as bioconvection. The density of suspended layer of microorganisms is greater than that of water and can be easily observed at the boundary. Nowadays there are many researchers who investigate the improvement of transfer rate of mass and the species concentration because of its importance in different industries such as the making of polymer sheets, the process of conveyor belt, chemical process, applications of biotechnology, etc. Shafiq et al. (2020) used convective boundary conditions to check the qualities of bioconvective tangent hyperbolic fluid flow on a moving surface. In this study, they discussed local motile microbes. The susceptibility to Brownian motion constant is lowered despite an increment in the Brownian motion factor. Hosseinzadeh et al. (2020) studied nanobioconvective fluid flow with gyrotactic microorganisms in the presence of radiation and discussed that when Brownian motion is extended from 0.1 to 0.9, the nondimensional temperature goes up by 31.7 percent. Furthermore, boosting the bioconvection Schmidt coefficient from 0.1 to 2 minimizes the nondimensional microbe pattern by more than four times. Mondal and Pal (2020) numerically investigated bioconvective flow with motile microorganisms past over a stretch wedge with a porous matrix. This study elaborates that temperature dispersion expands more in the presence of nonlinear thermal radiation compared to linear thermal energy. Ferdows et al. (2020) discussed the flow of gyrotactic microorganisms over an exponentially moving sheet. Abdal et al. (2021a) evaluated the radiation and multiple slip impacts on magnetohydrodynamic bioconvection stream of a micropolar nanofluid across an extending surface employing the fourth-order Runge–Kutta method with shooting approach. In Abdal et al. (2015), Ali et al. (2019a), Habib et al. (2021), distinct flow features of micropolar fluid are deliberated.

Nanofluids show different characteristics due to which their are convenient to use in many applications such as fuel cells, processes of pharmaceuticals, engines having hybrid power, etc. Nanoparticles behave like a link between atomic structures and bulk materials. Nanofluids are involved in biomedical applications, for example, separation of magnetic

cells, delivery of drugs, cry prevention, etc. Rashid et al. (2020) studied the effects of different shape nanoparticles by using entropy generation. The outcomes reveal that lamina-shaped nanomaterials improve performance in temperature dispersion, heat exchange, and entropy formation. Narender et al. (2020) studied nanofluids and Casson fluid flows with stagnation point by using a radial sheet. The findings showed that the radiation variable is elevated in a Casson nanofluid and the heat transport coefficient is improved. Yahya et al. (2021a) analyzed thermal attributes of Williamson Sutterby nanofluid flow through a Darcy–Forchheimer spongy media across an extended surface while considering the Cattaneo–Christov heat transfer, radiation heat transfer coefficient, and convective boundary constraints. Ali et al. (2021c) employed a nonlinear finite element approach to investigate the dynamics of liquid transporting tiny particles, Coriolis force impacts, and Cattaneo–Christov heat flux on transient rotating flow toward a constantly expanding sheet. Jafar et al. (2020) discussed the flow of nanofluid across a nonlinear sheet. This work demonstrates that the solid density of nanoparticles can be used to influence heat transmission and nanofluid stream patterns. Ali et al. (2020b) used the variational finite element procedure to examine the effect of a gravitational dipole on the heat transmission occurrences of distinct nanoparticles Fe (ferromagnetic) and  $\text{Fe}_3\text{O}_4$  (ferrimagnetic) dissipated in a base liquid (60% water + 40% ethylene glycol) on micropolar fluid stream over an elongating sheet.

In different industries and technologies, there are multiple usages of non-Newtonian fluids such as Maxwell fluids. Some applications are paints, production of cosmetics, suspensions, different oils, solutions of polymers, etc. To show the behavior of viscoelastic in any fluid, the model of Maxwell fluid is very useful. Graphene Maxwell nanofluid flow moving over a horizontal sheet with slip conditions was presented by Hussain et al. (2020b). The findings suggest that the graphene Maxwell nanofluid velocity drops when the magnetic flux, the inclination angle of the magnetic flux, permeability, and unsteadiness variables increase; however, the trend of the fluid velocity alters as the Maxwell factor improves. Ali et al. (2020a) discussed heat effects in Maxwell nanofluid flow passing above the wedge. The higher the Hartmann quantity  $Ha$ , unstable parameter  $A$ , Deborah factor  $\beta$ , and wedge parameter  $m$ , the quicker the stream down the wall and the thinner the boundary layer. Ahmed et al. (2020) presented the study of unsteady flow of Maxwell nanofluid over a stretched cylinder. The conclusions indicate that when the unsteadiness variable, curvature parameter, and Maxwell parameter are improved, so are the temperature and concentration pattern. Irfan et al. (2020) considered chemical reaction along with heat for Maxwell nanofluid flow. Devi and Mabood (2020) elaborated the numerical study of Margoni Maxwell and nanofluid flow. Ramesh et al. (2020) discussed Maxwell nanofluid flow and extended the magnetohydrodynamics and radiation effects by using the Riga plate.

Khan et al. (2020) investigated the Cattaneo–Christov fluid and nanofluid. Ali et al. (2020c) analyzed the effects of Stefan blasting on Cattaneo–Christov features and bioconvection of self-motivated microbes dispersed in water-based nanoparticles with a guiding edge ablation/accretion employing the finite element approach. Abid et al. (2020) discussed the heat flux of Cattaneo–Christov fluid along with the nanofluids. He discussed his observations under the action of copper oxide water and ionized copper that is partially magnetized. Sha et al. (2019) discussed the impact of Hall on the heat flux of Cattaneo–Christov flow and the nanofluid couple stress, which is three-dimensional, passed on a stretching sheet. It is observed that elevating the thermal relaxation variable, the Prandtl number and temperature coefficient diminishes the temperature profile. Shah et al. (2019) investigated the Casson ferrofluids along with micropolar fluids having thermal conductivity and a model of Cattaneo–Christov on a stretching sheet. The observations suggest that greater  $EI$  and

$K$  enhance velocity, whereas lowering  $\beta$  and  $M$  quantities diminishes flow motion, and rising  $K$  values improves microrotation pattern, whereas reducing  $\beta$  values lower microrotation profile. Abdal et al. (2021b) investigated the mass transportation and heat conduction of stagnation point circulation of Casson nanofluid via permeable matrix controlled by a consistent intensity magnetic field across an expanding cylindrical surface. Ali et al. (2021b) adopted the Buongiorno theory and the finite element methodology to examine the time-dependent revolving magnetic transportation of a water base fluid  $H_2O$  with hybrid nanoparticles  $Al_2O_3 - Cu$  and  $Al_2O_3 - TiO_2$  across an expanding sheet. Abdal et al. (2021c) explored the consequences of bioconvection and activation heat on Reiner–Rivlin nanofluid transport on a rotating disc having partial slips adopting the Runge–Kutta fourth-order technique and the shooting methodology. Diverse applications of nanofluids in various aspects are examined by some other scholars (Ali et al. 2021a; Yahya et al. 2021b; Habib et al. 2022; Ahmad et al. 2021).

In the last few decades, many researchers have shown their interest in the flow of magneto-hydrodynamics (MHD) for the fluids, which are good conductors of electricity over a heated surface, and its usage in various problems of engineering, for example, control of boundary layer in aerodynamics, cooling in nuclear reactors, petroleum industries, etc. Jabeen et al. (2020) analyzed the comparative analysis for MHD with radiation in a porous matrix. Observe that for different Newtonian and non-Newtonian liquids, the thermal and concentration patterns of MHD flow of Maxwell fluid are significantly affected. Fractional heating effects with a linear sheet for MHD boundary layer flow were analyzed by Shanappa et al. (2020). It is well understood that  $Nt$  is an increasing factor of both thermal and solutal transportation vectors. Panigrahi et al. (2020) discussed the effects of mass and heat transfer for MHD with Casson nanofluid flows over a stretch sheet. They elaborate that the consequences of a changeable magnetic field are being extensively employed in many engineering implementations such as magneto-hydrodynamic (MHD) propelling forces, speed of cooling, MHD power production, etc. Abdal et al. (2020) studied the multislip influences on the magneto-hydrodynamic (MHD) mixed convective unsteady stream of micropolar nanofluids across an elongating/dwindling sheet in the existence of a source of heat by applying the Runge–Kutta fourth-order approach with shooting strategy. Hussain et al. (2020a) used the Runge–Kutta technique to examine the boundary layer stream and heat transmission features of an MHD nanofluid across a permeable plate involving thermal radiation. Ali et al. (2020d) explored unstable magneto-hydrodynamic (MHD) nanoparticles circulation across a radially nonlinear stretchable sheet as well as temperature-dependent viscosity, convective boundary situation, thermodiffusion and thermal radiation. Abbas et al. (2019), Ali et al. (2019b) scrutinized the MHD flow attributes in distinct aspects.

After reviewing the past literature, we focused on the study of enhanced heat transportation of Maxwell nanofluids with activation energy. Bioconvection and Cattaneo–Christov flux over an extending sheet are taken into account. The very objective pertains to enhance thermal conductivity of the base fluid for efficient thermal transportation of compact density heat exchangers of modern thermal process. Graphical results are presented by using numerical simulation obtained by converting PDE into ODEs with suitable transformation. A comparison of current findings is made with already published related studies.

## 2 Physical model and mathematical formulation

Two-dimensional steady flow of Maxwell fluid along with mild inclusion of nanoparticles and gyrotactic microorganisms is considered. The incompressible flow through porous medium takes place due to stretching sheet. The stretching velocity of the sheet along the

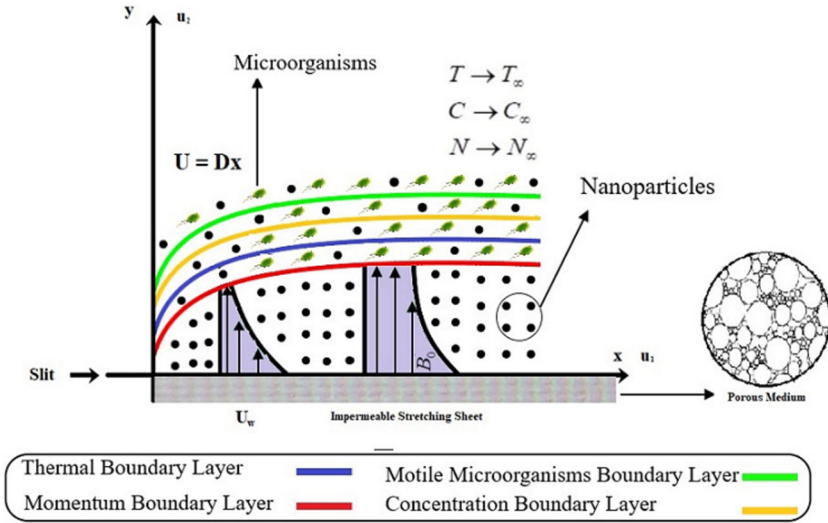


Fig. 1 Problem description

$x$ -axis is  $U_w$ . Due to the permeable stretching sheet, flow is generated linearly, where  $u_1$  and  $u_2$  are the velocities of fluid flow along the  $x$ -, and  $y$ -axes, respectively. In Fig. 1 the temperature, concentration of nanoparticles, and motile density of microorganisms are taken as  $T$ ,  $C$ , and  $N$ . The Cattaneo–Christov heat flux and activation energy are taken into account. Now our problem represents the basic equation of continuity, equation of momentum, energy equation, concentration equation, and gyrotactic microorganism equation in Cartesian coordinates. The following equations are established in the aspects of the flow of fluids (Dawar et al. 2021; Shahid 2020; Shahid et al. 2020, 2021):

$$\frac{\partial u_1}{\partial x} + \frac{\partial u_2}{\partial y} = 0, \quad (1)$$

$$u_1 \frac{\partial u_1}{\partial x} + u_2 \frac{\partial u_1}{\partial y} = v_{nf} \frac{\partial}{\partial y} \frac{\partial u_1}{\partial y} - \lambda(u_1^2 \frac{\partial^2 u_1}{\partial x^2} + u_2^2 \frac{\partial^2 u_1}{\partial y^2} + 2u_1 u_2 \frac{\partial^2 u_1}{\partial x \partial y}) - \frac{\sigma B_0^2 u_1}{\rho} - \frac{v_{nf}}{k_1} u_1 + \frac{1}{\rho}(\beta(1 - C_\infty)\rho g(T - T_\infty) - (\rho_p - \rho)g(C - C_\infty) - (N - N_\infty)g\gamma(\rho_m - \rho)), \quad (2)$$

$$u_1 \frac{\partial T}{\partial x} + u_2 \frac{\partial T}{\partial y} = \alpha \frac{\partial}{\partial y} \frac{\partial T}{\partial y} + \frac{\rho_p C_p}{\rho C} (D_B \frac{\partial C}{\partial y} \frac{\partial T}{\partial y} + \frac{D_T}{T_\infty} (\frac{\partial T}{\partial y})^2) + \tau_1 [u_1 \frac{\partial u_1}{\partial x} \frac{\partial T}{\partial x} + u_2 \frac{\partial u_2}{\partial x} \frac{\partial T}{\partial x} + u_1 \frac{\partial u_2}{\partial x} \frac{\partial T}{\partial x} + u_2 \frac{\partial u_1}{\partial y} \frac{\partial T}{\partial x} + 2u_1 u_2 \frac{\partial^2 T}{\partial x \partial y} + u_1^2 \frac{\partial}{\partial x} \frac{\partial T}{\partial x} + u_2^2 \frac{\partial}{\partial y} \frac{\partial T}{\partial y}], \quad (3)$$

$$u_1 \frac{\partial C}{\partial x} + u_2 \frac{\partial C}{\partial y} = D_B \frac{\partial}{\partial y} \frac{\partial C}{\partial y} + \frac{D_T}{T_\infty} \frac{\partial}{\partial y} \frac{\partial T}{\partial y} - (Kr)^2 (C_w - C_\infty) (\frac{T}{T_\infty})^m \exp(\frac{-E_a}{k_2 T}), \quad (4)$$

$$u_1 \frac{\partial N}{\partial x} + u_2 \frac{\partial N}{\partial y} = -bW_c \frac{\partial}{\partial y} (\frac{n}{\Delta C} \frac{\partial C}{\partial y}) + D_m \frac{\partial}{\partial y} \frac{\partial N}{\partial y}. \quad (5)$$

It is to mention that in Eq. (2),  $\lambda$  represents the Maxwell parameter when  $\lambda \neq 0$ ; otherwise, it is the Newtonian fluid  $\lambda = 0$ . The boundary conditions of the given problem are

$$\left. \begin{aligned} u_1 = U_w, u_2 = v_w, T = T_w, C = C_w, N = N_w, \text{ as } y = 0, \\ u \rightarrow 0, T \rightarrow T_\infty, C \rightarrow C_\infty, N \rightarrow N_\infty \text{ as } y \rightarrow \infty, \end{aligned} \right\} \quad (6)$$

$$\eta = \sqrt{\frac{D}{\nu}} y, u_1 = D_x f'(\eta), u_2 = -\sqrt{D\nu} f(\eta), \theta(\eta) = \frac{T - T_\infty}{T_w - T_\infty},$$

$$\phi(\eta) = \frac{C - C_\infty}{C_w - C_\infty}, \chi(\eta) = \frac{N - N_\infty}{N_w - N_\infty}. \quad (7)$$

$$f''' - f'^2 + ff'' - \beta(f^2 f''' - 2ff'f'') - (M + K_p)f' + \omega(\theta - Nr\phi - Rb\chi) = 0, \quad (8)$$

$$\theta'' + Prf\theta' + \frac{Nc}{Le}\theta'\phi' + \frac{Nc}{Le * Nbt}\theta'^2 + b(f^2\theta'' + ff'\theta') = 0, \quad (9)$$

$$\phi'' + Sc(f\phi') + \left(\frac{1}{Nbt}\right)\theta'' - Sc * A\phi(1 + \delta\theta)^n \exp\left(\frac{-E}{1 + \delta\theta}\right) = 0, \quad (10)$$

$$\chi'' + Lb(f\chi') - Pe[\phi''(\chi + \Omega) + \chi'\phi'] = 0. \quad (11)$$

$$\left. \begin{aligned} f(0) = H, f'(0) = 1, \theta(0) = 1, \phi(0) = 1, \chi(0) = 1, \text{ at } \eta = 0, \\ f'(\infty) \rightarrow 0, \theta(\infty) \rightarrow 0, \phi(\infty) \rightarrow 0, \chi(\infty) \rightarrow 0, \text{ as } \eta \rightarrow \infty. \end{aligned} \right\} \quad (12)$$

The nondimensional parameters are defined as

$$M = \frac{\sigma B_0^2}{D\rho}, K_p = \frac{\nu_{nf}}{k_1 D}, \omega = \frac{Gr}{Re_x^2}, Nr = \frac{Gr^*}{Gr}, Rb = \frac{(\rho_m - \rho)\gamma N_\infty}{(1 - C_\infty)\rho\beta T_\infty}, Pr = \frac{\nu_{nf}}{\alpha}, Nc = \frac{\rho_p C_p}{\rho C} (C_w - C_\infty), Le = \frac{\alpha}{D_B}, Nbt = \frac{D_B T_\infty (C_w - C_\infty)}{D_T (T_w - T_\infty)}, b = \tau_1 D, Sc = \frac{\nu_{nf}}{D_B}, A = \frac{k^2 r}{D}, \delta = \frac{T_w - T_\infty}{T_\infty}, E = \frac{E_a}{k_2 T_\infty}, Lb = \frac{\nu_{nf}}{D_m}, Pe = \frac{b_1 Wc}{k}, \Omega = \frac{N_\infty}{N_w - N_\infty}, H = \frac{-\nu_w}{\sqrt{D\nu_{nf}}}, \text{ and } \beta = \lambda D.$$

The physical quantities of interest such as  $Cf_x$  (skin friction coefficient),  $Nu_x$  (local Nusselt number),  $Sh_x$  (local Sherwood number), and  $Nn_x$  (local density of microorganism) are given as follows:

$$Cf_x = \frac{\tau_w}{(\rho U_w)^2}, Nu_x = \frac{xq_w}{k(T_w - T_\infty)}, Sh_x = \frac{xq_m}{D_B(C_w - C_\infty)}, Nn_x = \frac{xq_n}{D_m(N_w - N_\infty)},$$

where  $\tau_w$ ,  $q_w$ ,  $q_m$ , and  $q_n$  denote the shear stress, surface heat flux, surface mass flux, and motile microorganism flux given (at  $y = 0$ ) as

$$\tau_w = \mu(1 + \beta)\frac{\partial u}{\partial y}, q_w = -K\frac{\partial T}{\partial y}, q_m = -D_B\frac{\partial C}{\partial y}, q_n = -D_m\frac{\partial N}{\partial y}.$$

Solving these quantities with the help of given similarity transformation, we obtain

$$Cf_x(Re_x)^{-1/2} = f''(0), Nu_x(Re_x)^{-1/2} = -\theta'(0), Sh_x(Re_x)^{-1/2} = -\phi'(0), Nn_x(Re_x)^{-1/2} = -\chi'(0).$$

where  $(Re_x) = \frac{xU_w}{\nu}$  is the local Reynolds number.

### 3 Numerical procedure

In this segment, numerical results from the resulting dimensionless nonlinearly coupled ordinary differential equations Eqs. (8)–(11) with boundary conditions Eq. (12) are obtained by the fourth-order Runge–Kutta method. The nonlinear characteristics of these equations create a serious hurdle to yield any exact solution to such problems. There are several numerical procedures involving arbitrary parameters or discretizations. Such schemes are laborious. The Runge–Kutta method is simple, economic, and easily coded. It provides an



**Table 1** The comparative outputs for  $-\theta'(0)$

$Pr$	Goyal and Bhargava (2014)	Nadeem and Hussain (2014)	Present results
0.2	0.1691	0.169	0.1694
0.7	0.4539	0.454	0.4538
2.0	0.9113	0.911	0.9102
7.0	1.8954	-	1.8943
20.0	3.3539	-	3.3528

accuracy of  $o(h^5)$ . The far-off boundary is  $\eta \rightarrow \infty$ ; we replace it by  $\eta = 4.5$  (for velocity profile) and  $\eta = 9$  (for temperature and concentration profiles). The method provides reliable fast convergence during the sizable variation of controlling parameters. To execute this numerical method, the differential Eqs. (8)–(11) are transformed into a first-order system with the implementation of new variables

$$\begin{aligned}
 s_1' &= s_2, \\
 s_2' &= s_3, \\
 s_3' &= s_2^2 - s_1 s_3 + \beta(s_1^2 ds_3 - 2s_1 s_2 s_3) + (M + Kp)s_2 - \omega(s_4 - Nr s_6 - Rb s_8), \\
 s_4' &= s_5, \\
 s_5' &= -Pr s_1 s_5 - \frac{Nc}{Le} s_5 s_7 - \frac{Nc}{Le * Nbt} s_5^2 - b(s_1^2 ds_5 + s_1 s_2 s_5), \\
 s_6' &= s_7, \\
 s_7' &= -Sc s_1 s_7 - \frac{1}{Nbt} ds_5 + Sc * A[1 + \delta s_6]^n \exp\left[\frac{-E}{1 + \delta s_6}\right] s_8, \\
 s_8' &= s_9, \\
 s_9' &= -Lb s_1 s_9 + Pe[s_7 s_9 + (\Omega + s_8) ds_7],
 \end{aligned}$$

along with the boundary conditions

$$\begin{aligned}
 s_1 = H, s_2 = 1, s_4 = 1, s_6 = 1, s_8 = 1 \text{ at } \eta = 0, \text{ and} \\
 s_2 \rightarrow 0, s_4 \rightarrow 0, s_6 \rightarrow 0, s_8 \rightarrow 0 \text{ as } \eta \rightarrow \infty.
 \end{aligned}$$

## 4 Results and discussion

In this part, we presented and explained the outcomes computed from the above-mentioned procedure. The validation of current results is established when these are compared with the existing findings of Goyal and Bhargava (2014), Nadeem and Hussain (2014) in limiting cases. The three sets of results in Table 1 show a close agreement.

Extensive computational endeavor is made to assess the influences of pertinent parameters on the dependent quantities to inspect the physical nature of the work. The evaluations are made for three cases of mass transpiration parameter  $H$  ( $H = -ve$ ,  $H = 0$ ,  $H = +ve$ ). Table 2 indicates that the drag force is supplemented with an incremental variation of  $M$ ,  $K_p$ ,  $Nr$ ,  $Rb$ ,  $\beta$ , and hence the magnitude of  $-f''(0)$  (skin friction factor) is enhanced because the additional resistance to the flow comes into play. However, the skin friction is reciprocated against mixed convection parameter  $\omega$ , because the rise in mixed convection helps to accelerate the flow. Table 3 shows that the Nusselt number  $-\theta'(0)$  improves in direct relation to  $Pr$ ,  $Le$ ,  $Nbt$ , and  $b$ , but it diminishes against  $Nc$ . Table 4 convinces that  $-\phi'(0)$  recedes only as  $E$  rises, whereas  $-\phi'(0)$  is upsurged directly with  $Sc$ ,  $A$ ,  $\delta$ , and  $n$ . From Table 5 we notice that the magnitude of motile density  $-\chi'(0)$  increases when  $Lb$ ,  $Pe$ , and  $\Omega$  are uplifted.

Figure 2 exhibits the variation of velocity  $f'(\eta)$  under the effects of  $M$  and  $K_p$ . The deceleration in the flow against  $M$  is due to Lorentz's force, which comes into play due to

**Table 2** Results for  $-f''(0)$

$M$	$Kp$	$\omega$	$Nr$	$Rb$	$\beta$	$H = -0.1$	$H = 0$	$H = 0.1$
0.1	0.5	0.1	0.1	0.1	0.5	1.5126	1.5872	1.6757
0.3						1.5903	1.6640	1.7518
0.5						1.6637	1.7367	1.8240
0.5	0.1					1.5126	1.5872	1.6757
	0.5					1.6637	1.7367	1.8240
	1.0					1.8328	1.9042	1.9904
	0.5	0.1				1.6637	1.7367	1.8240
		0.2				1.6105	1.6832	1.7700
		0.3				1.5592	1.6316	1.7178
		0.1	0.1			1.6637	1.7367	1.8240
			0.2			1.6689	1.7419	1.8293
			0.3			1.6741	1.7471	1.8346
			0.1	0.1		1.6637	1.7367	1.8240
				0.2		1.6676	1.7404	1.8276
				0.3		1.6714	1.7441	1.8312
				0.1	0.1	1.3828	1.4364	1.4938
					0.3	1.5205	1.5835	1.6549
					0.5	1.6637	1.7367	1.8240

**Table 3** Results for  $-\theta'(0)$

$Pr$	$Nc$	$Le$	$Nbt$	$b$	$-\theta'(0)$
0.71	0.5	4.0	2.0	0.5	0.4885
1.0					0.5296
2.0					0.8962
0.71	0.1				0.4443
	0.5				0.4085
	1.0				0.3673
	0.5	2.0			0.3714
		4.0			0.4085
		6.0			0.4222
		4.0	2.0		0.4085
			3.0		0.4120
			4.0		0.4137
			2.0	0.1	0.3806
				0.5	0.4085
				1.0	0.4453

the interaction of magnetic and electric fields; also, the resistive nature of the porous matrix represented by  $K_p$  is responsible to slow the velocity. Moreover, injection accelerates the flow as compared to suction. In Fig. 3 the mixed convection parameter  $\omega$  causes an increment in the flow velocity, whereas the higher inputs of buoyancy ratio parameter  $Nr$  and bioconvection Raleigh number  $Rb$  depreciate  $f'(\eta)$ . To increase  $Rb$ , the buoyancy force is

**Table 4** Results for  $-\phi'(0)$

$Sc$	$A$	$\delta$	$n$	$E$	$-\phi'(0)$
1.0	0.1	0.1	0.5	0.3	0.7333
2.0					1.0157
3.0					1.2887
1.0	0.1				0.7333
	0.2				0.9508
	0.3				1.1222
	0.1	0.1			0.7333
		0.2			0.7461
		0.3			0.7583
		0.1	0.1		0.7263
			0.5		0.7333
			1.0		0.7422
			0.5	0.3	0.7333
				0.7	0.6476
				1.0	0.5953

**Table 5** Results for  $-\chi'(0)$

$Lb$	$Pe$	$\Omega$	$-\chi'(0)$
1.2	1.2	0.2	1.5411
2.0			1.8001
3.0			2.0876
1.2	0.2		0.7756
	1.2		1.5411
	2.0		2.1758
	1.2	0.2	1.5411
		0.4	1.6868
		0.6	1.8323

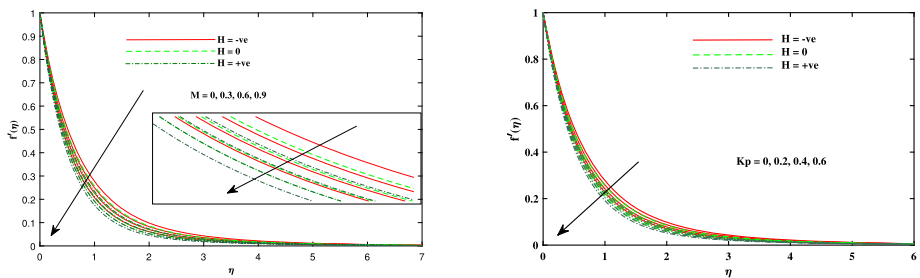


**Fig. 2** Plot for velocity profile  $f'(\eta)$  with varying values of  $M$  and  $K_p$

increased, due to which the velocity of the fluid is decelerated. From Fig. 4 we see that the temperature  $\theta(\eta)$  rises directly with  $M$ , but it declines against the Cattaneo–Christov parameter  $b$ . The dragging of fluid in the boundary layer region due to Lorentz forces resulted

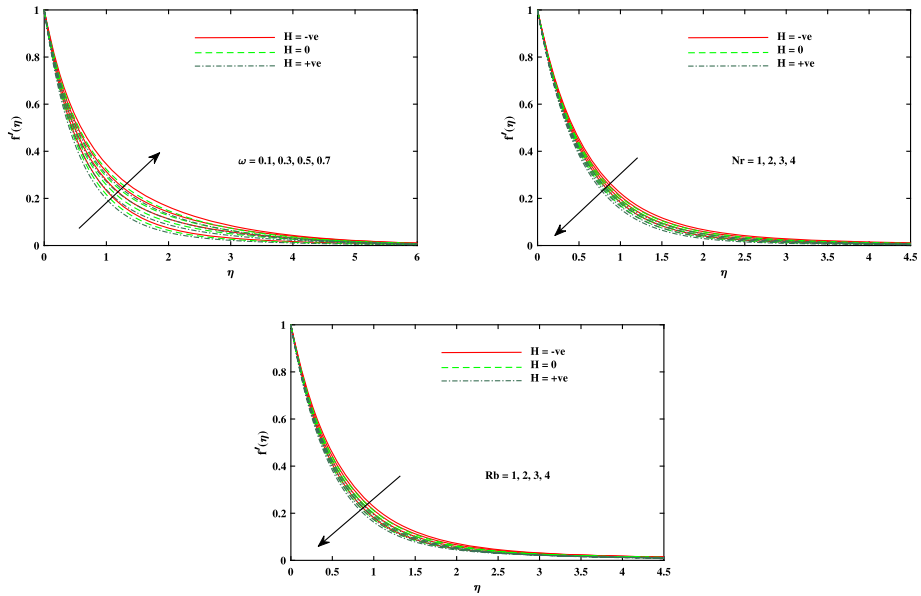


Fig. 3 Plot for temperature profile  $f'(\eta)$  with varying values of  $\omega$ ,  $Nr$ , and  $Rb$

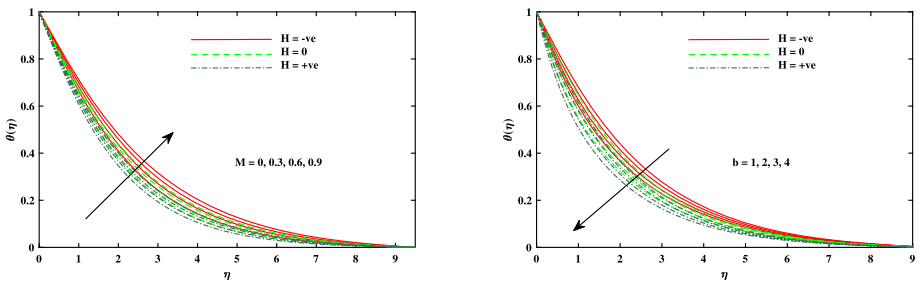


Fig. 4 Plot for velocity profile  $\theta(\eta)$  with varying values of  $M$  and  $b$

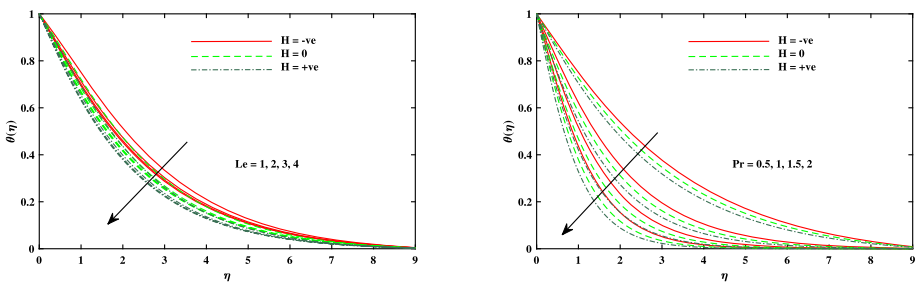
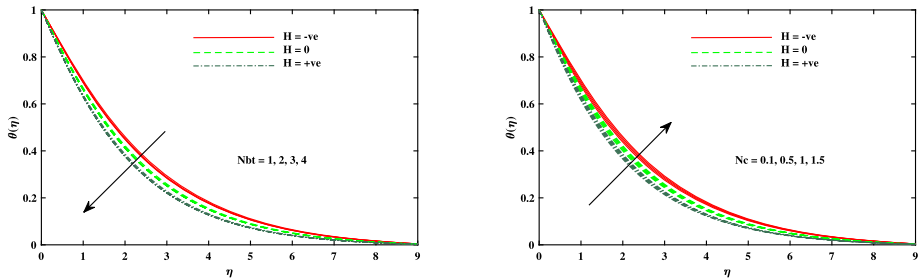
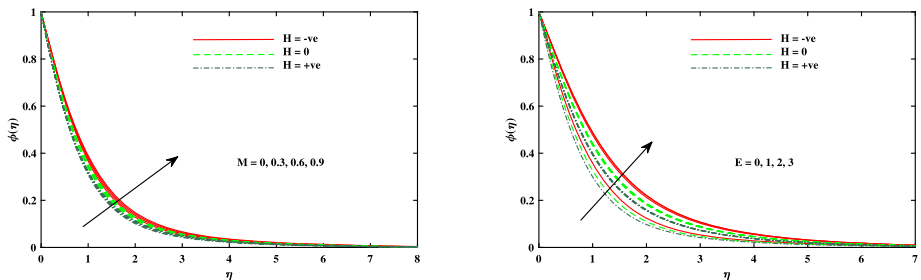


Fig. 5 Plot for velocity profile  $\theta(\eta)$  with varying values of  $Le$  and  $Pr$



**Fig. 6** Plot for velocity profile  $\theta(\eta)$  with varying values of  $Nbt$  and  $Nc$



**Fig. 7** Plot for velocity profile  $\phi(\eta)$  with varying values of  $M$  and  $E$

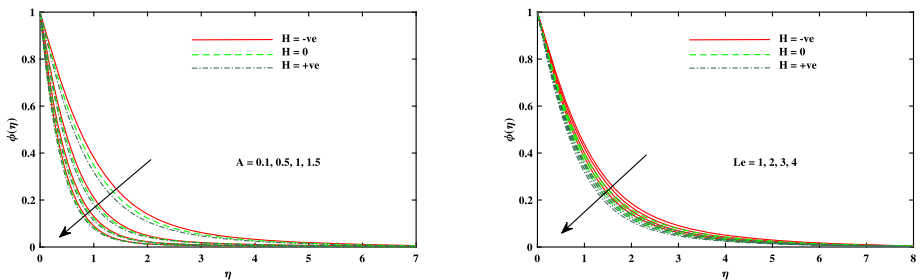


**Fig. 8** Plot for velocity profile  $\phi(\eta)$  with varying values of  $A$  and  $Le$

in thermal dissipation to produce extra heat in this region, and hence the fluid temperature increases with  $M$ . Figure 5 sketches the decrement in  $\theta(\eta)$  against the Lewis number  $Le$  and Prandtl number  $Pr$ . Decrement shows in  $\theta(\eta)$  the rising values of  $Le$ , and  $Pr$  is reciprocated to thermal diffusivity. Figure 6 delineates decreasing patterns of  $\theta(\eta)$  against Brownian motion parameter  $Nbt$  but its rising behavior with  $Nc$ . From Fig. 7 we notice that the concentration profile  $\phi(\eta)$  rises with the higher inputs of  $M$  and  $E$ . Physically, the rise in species concentration in the solutal boundary layer with incremented  $M$  is attributed to the higher diffusion in this region. Whereas  $\phi(\eta)$  diminishes against larger values of the chemical reaction rate parameter  $A$  and Lewis number  $Le$ , as we notice in Fig. 8. The higher chemical reaction rate is responsible to lower the concentration, and larger  $Le$  means lesser mass diffusivity. Figure 9 exhibits that the nanoparticle concentration declines against

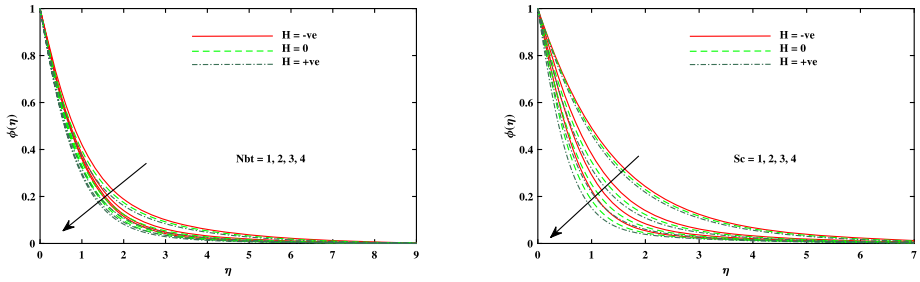


**Fig. 9** Plot for velocity profile  $\phi(\eta)$  with varying values of  $Nbt$  and  $Sc$

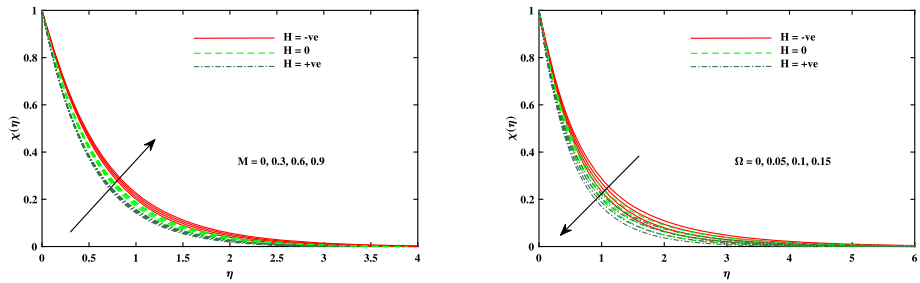


**Fig. 10** Plot for velocity profile  $\xi(\eta)$  with varying values of  $M$  and  $\Omega$

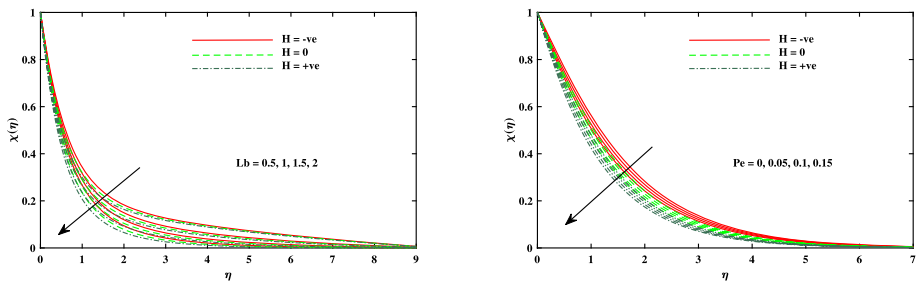


**Fig. 11** Plot for velocity profile  $\xi(\eta)$  with varying values of  $Lb$  and  $Pe$

$Nbt$  and  $Sc$  (for  $Nbt$ , see Dawar et al. 2021). Figure 10 is drawn to depict that the motile density profile  $\chi(\eta)$  is progressed when  $M$  is incremented, and it declines when values of microorganism the difference parameter  $\Omega$  are boosted. A depreciation in motile density profile against the incremented value of bioconvection Lewis number  $Lb$  and  $Pe$  is noticed, as depicted in Fig. 11. Physically, it illustrates that the microorganism profile is enhanced while escalating the bioconvection Peclet number  $Pe$ . Whereas  $Pe$  contains interrelation by means of maximum cell swimming movement, chemotaxis is constant and has the opposite relationship in the diffusivity of the microorganism. As a result, for higher values of  $Pe$ , the microorganisms profile is raised up.

## 5 Conclusions

The study elaborates the effects of heat transportation for the bioconvective motion of Maxwell nanofluids over an extending sheet with Cattaneo–Christov flux along with activation energy and mass transpiration. The fluid flow, heat, and mass transport take place due to stretch in the horizontal sheet. The main focus is to enhance the thermal conductivity of base fluid when nano-sized material is homogeneously mixed. The important outputs of this study are summarized as follows:

- The bulk flow velocity  $f'(\eta)$  shows decrement behavior when the values of  $M$ ,  $Kp$ ,  $Nr$ , and  $Rb$  increase, but velocity increases with increasing values of  $\omega$ .
- The temperature profile  $\theta(\eta)$  goes up when  $M$  and  $Nc$  uplift, but it decreases rapidly when  $b$ ,  $Pr$ ,  $Le$ , and  $Nbt$  lift up.
- The concentration profile  $\phi(\eta)$  shows decreasing behavior for  $A$ ,  $Le$ ,  $Nbt$ , and  $Sc$ , but for  $M$  and  $E$ , the concentration increases.
- Motile density profile of microorganisms  $\chi(\eta)$  slows down with the rising values of  $\Omega$ ,  $Lb$ , and  $Pe$ , whereas it expressed an increment due to increase in  $M$ .
- The skin friction factor goes upward rapidly with  $M$ ,  $Kp$ ,  $Nr$ ,  $Rb$ ,  $\beta$ , whereas it moves in the opposite direction for higher inputs of  $\omega$ .
- $Pr$ ,  $Nbt$ ,  $b$ , and  $Le$  increase the Nusselt number  $-\theta'(0)$ , but  $Nc$  reduces it when these parameters take higher values.
- The Sherwood number  $-\phi'(0)$  uplifts with  $Sc$ ,  $A$ ,  $\delta$ , and  $n$ , but shows the opposite behavior against  $E$ .
- The motile density number  $-\chi'(0)$  increases for  $Lb$ ,  $\Omega$ , and  $Pe$ .

**Authors' Contribution** Each of the authors contributed equally to each part of this work. All authors read and approved the final manuscript.

**Funding** N/A.

**Data Availability** All data generated or analyzed during this study are included in this paper.

## Declarations

**Competing interests** The authors declare that they have no competing interests.

## References

- Abbas, Z., Abdal, S., Hussain, N., Hussain, F., Adnan, M., Ali, B., Zulqarnain, R.M., Ali, L., Younas, S.: MHD boundary layer flow and heat transfer of nanofluid over a vertical stretching sheet in the presence of a heat source. *Sci. Inq. Rev.* **3**(4), 60–73 (2019)
- Abdal, S., Hussain, S., Ahmad, F., Ali, B.: Hydromagnetic stagnation point flow of micropolar fluids due to a porous stretching surface with radiation and viscous dissipation effects. *Sci. Int.* **27**, 3965–3971 (2015)
- Abdal, S., Ali, B., Younas, S., Ali, L., Mariam, A.: Thermo-diffusion and multislip effects on MHD mixed convection unsteady flow of micropolar nanofluid over a shrinking/stretching sheet with radiation in the presence of heat source. *Symmetry* **12**(1), 49 (2020)
- Abdal, S., Alhumade, H., Siddique, I., Alam, M.M., Ahmad, I., Hussain, S.: Radiation and multiple slip effects on magnetohydrodynamic bioconvection flow of micropolar based nanofluid over a stretching surface. *Appl. Sci.* **11**(11), 5136 (2021a)
- Abdal, S., Hussain, S., Siddique, I., Ahmadian, A., Ferrara, M.: On solution existence of MHD Casson nanofluid transportation across an extending cylinder through porous media and evaluation of priori bounds. *Sci. Rep.* **11**(1), 1–16 (2021b)

- Abdal, S., Mariam, A., Ali, B., Younas, S., Ali, L., Habib, D.: Implications of bioconvection and activation energy on Reiner–Rivlin nanofluid transportation over a disk in rotation with partial slip. *Chin. J. Phys.* **73**, 672–683 (2021c)
- Abid, N., Ramzan, M., Chung, J.D., Kadry, S., Chu, Y.-M.: Comparative analysis of magnetized partially ionized copper, copper oxide–water and kerosene oil nanofluid flow with Cattaneo–Christov heat flux. *Sci. Rep.* **10**(1), 1–14 (2020)
- Ahmad, F., Abdal, S., Ayed, H., Hussain, S., Salim, S., Almatroud, A.: The improved thermal efficiency of Maxwell hybrid nanofluid comprising of graphene oxide plus silver/kerosene oil over stretching sheet. *Case Stud. Therm. Eng.* **27**, 101257 (2021)
- Ahmed, A., Khan, M., Hafeez, A., Ahmed, J.: Thermal analysis in unsteady radiative Maxwell nanofluid flow subject to heat source/sink. *Appl. Nanosci.* **10**, 5489–5497 (2020)
- Ali, L., Liu, X., Ali, B., Mujeed, S., Abdal, S.: Finite element simulation of multi-slip effects on unsteady mhd bioconvective micropolar nanofluid flow over a sheet with solutal and thermal convective boundary conditions. *Coatings* **9**(12), 842 (2019a)
- Ali, L., Liu, X., Ali, B., Mujeed, S., Abdal, S.: Finite element analysis of thermo-diffusion and multi-slip effects on MHD unsteady flow of Casson nano-fluid over a shrinking/stretching sheet with radiation and heat source. *Appl. Sci.* **9**(23), 5217 (2019b)
- Ali, B., Hussain, S., Nie, Y., Khan, S.A., Naqvi, S.I.R.: Finite element simulation of bioconvection Falkner–Skan flow of a Maxwell nanofluid along with activation energy over a wedge. *Phys. Scr.* **95**(9), 095214 (2020a)
- Ali, L., Liu, X., Ali, B., Mujeed, S., Abdal, S., Khan, S.A.: Analysis of magnetic properties of nano-particles due to a magnetic dipole in micropolar fluid flow over a stretching sheet. *Coatings* **10**(2), 170 (2020b)
- Ali, L., Liu, X., Ali, B., Mujeed, S., Abdal, S., Mutahir, A.: The impact of nanoparticles due to applied magnetic dipole in micropolar fluid flow using the finite element method. *Symmetry* **12**(4), 520 (2020c)
- Ali, B., Naqvi, R.A., Nie, Y., Khan, S.A., Sadiq, M.T., Rehman, A.U., Abdal, S.: Variable viscosity effects on unsteady MHD an axisymmetric nanofluid flow over a stretching surface with thermo-diffusion: FEM approach. *Symmetry* **12**(2), 234 (2020d)
- Ali, B., Ali, L., Abdal, S., Asjad, M.I.: Significance of Brownian motion and thermophoresis influence on dynamics of Reiner–Rivlin fluid over a disk with non-Fourier heat flux theory and gyrotactic microorganisms: a numerical approach. *Phys. Scr.* **96**(9), 094001 (2021a)
- Ali, B., Naqvi, R.A., Ali, L., Abdal, S., Hussain, S.: A comparative description on time-dependent rotating magnetic transport of a water base liquid H<sub>2</sub>O with hybrid nano-materials Al<sub>2</sub>O<sub>3</sub>-Cu and Al<sub>2</sub>O<sub>3</sub>-TiO<sub>2</sub> over an extending sheet using Buongiorno model: finite element approach. *Chin. J. Phys.* **70**, 125–139 (2021b)
- Ali, B., Nie, Y., Hussain, S., Habib, D., Abdal, S.: Insight into the dynamics of fluid conveying tiny particles over a rotating surface subject to Cattaneo–Christov heat transfer, Coriolis force, and Arrhenius activation energy. *Comput. Math. Appl.* **93**, 130–143 (2021c)
- Dawar, A., Shah, Z., Islam, S.: Mathematical modeling and study of MHD flow of Williamson nanofluid over a nonlinear stretching plate with activation energy. *Heat Transf.* **50**(3), 2558–2570 (2021)
- Devi, S.S.U., Mabood, F.: Entropy anatomization on Marangoni Maxwell fluid over a rotating disk with nonlinear radiative flux and Arrhenius activation energy. *Int. Commun. Heat Mass Transf.* **118**, 104857 (2020)
- Ferdows, M., Zaimi, K., Rashad, A.M., Nabwey, H.A.: MHD bioconvection flow and heat transfer of nanofluid through an exponentially stretchable sheet. *Symmetry* **12**(5), 692 (2020)
- Goyal, M., Bhargava, R.: Boundary layer flow and heat transfer of viscoelastic nanofluids past a stretching sheet with partial slip conditions. *Appl. Nanosci.* **4**(6), 761–767 (2014)
- Habib, D., Abdal, S., Ali, R., Baleanu, D., Siddique, I.: On bioconvection and mass transpiration of micropolar nanofluid dynamics due to an extending surface in existence of thermal radiations. *Case Stud. Therm. Eng.* **27**, 101239 (2021)
- Habib, D., Salamat, N., Abdal, S., Siddique, I., Ang, M.C., Ahmadian, A.: On the role of bioconvection and activation energy for time dependent nanofluid slip transpiration due to extending domain in the presence of electric and magnetic fields. *Ain Shams Eng. J.* **13**(1), 101519 (2022)
- Hosseinzadeh, K., Salehi, S., Mardani, M., Mahmoudi, F., Waqas, M., Ganji, D.: Investigation of nano-bioconvective fluid motile microorganism and nanoparticle flow by considering mhd and thermal radiation. *Inform. Med. Unlocked* **21**, 100462 (2020)
- Hussain, F., Abdal, S., Abbas, Z., Hussain, N., Adnan, M., Ali, B., Zulqarnain, R.M., Ali, L., Younas, S.: Buoyancy effect on MHD slip flow and heat transfer of a nanofluid flow over a vertical porous plate. *Sci. Inq. Rev.* **4**(1), 01 (2020a)
- Hussain, S.M., Sharma, R., Mishra, M.R., Alrashidy, S.S.: Hydromagnetic dissipative and radiative graphene Maxwell nanofluid flow past a stretched sheet-numerical and statistical analysis. *Mathematics* **8**(11), 19–29 (2020b)



- Irfan, M., Khan, M., Khan, W.: Heat sink/source and chemical reaction in stagnation point flow of Maxwell nanofluid. *Appl. Phys. A* **126**(11), 1–8 (2020)
- Jabeen, K., Mushtaq, M., Akram Muntazir, R.: Analysis of MHD fluids around a linearly stretching sheet in porous media with thermophoresis, radiation, and chemical reaction. *Math. Probl. Eng.* **2020**, 9685482 (2020)
- Jafar, A.B., Shafie, S., Ullah, I.: Mhd radiative nanofluid flow induced by a nonlinear stretching sheet in a porous medium. *Heliyon* **6**(6), e04201 (2020)
- Khan, M.I., Alzahrani, F., Hobiny, A., Ali, Z.: Modeling of Cattaneo–Christov double diffusions (CCDD) in Williamson nanomaterial slip flow subject to porous medium. *J. Mater. Res. Technol.* **9**(3), 6172–6177 (2020)
- Mondal, S.K., Pal, D.: Gyrotactic mixed bioconvection flow of a nanofluid over a stretching wedge embedded in a porous media in the presence of binary chemical reaction and activation energy. *Int. J. Ambient Energy* (2020). <https://doi.org/10.1080/01430750.2020.1814860>
- Nadeem, S., Hussain, S.: Flow and heat transfer analysis of Williamson nanofluid. *Appl. Nanosci.* **4**(8), 1005–1012 (2014)
- Narender, G., Govardhan, K., Sarma, G.S.: Magnetohydrodynamic stagnation point on a Casson nanofluid flow over a radially stretching sheet. *Beilstein J. Nanotechnol.* **11**(1), 1303–1315 (2020)
- Panigrahi, L., Panda, J., Swain, K., Dash, G.C.: Heat and mass transfer of MHD Casson nanofluid flow through a porous medium past a stretching sheet with Newtonian heating and chemical reaction. *Karbala Int. J. Mod. Math. Sci.* **6**(3), 11 (2020)
- Ramesh, K., Khan, S.U., Jameel, M., Khan, M.I., Chu, Y.-M., Kadry, S.: Bioconvection assessment in Maxwell nanofluid configured by a Riga surface with nonlinear thermal radiation and activation energy. *Surf. Interfaces* **21**, 100749 (2020)
- Rashid, U., Baleanu, D., Iqbal, A., Abbas, M.: Shape effect of nanosize particles on magnetohydrodynamic nanofluid flow and heat transfer over a stretching sheet with entropy generation. *Entropy* **22**(10), 1171 (2020)
- Sha, Z., Dawar, A., Alzahrani, E.O., Kumam, P., Khan, A.J., Islam, S.: Hall effect on couple stress 3D nanofluid flow over an exponentially stretched surface with Cattaneo Christov heat flux model. *IEEE Access* **7**, 64844–64855 (2019)
- Shafiq, A., Sindhu, T.N., Khaliq, C.M.: Numerical investigation and sensitivity analysis on bioconvective tangent hyperbolic nanofluid flow towards stretching surface by response surface methodology. *Alex. Eng. J.* (2020). <https://doi.org/10.1016/j.aej.2020.08.007>
- Shah, Z., Dawar, A., Khan, I., Islam, S., Ching, D.L.C., Khan, A.Z.: Cattaneo–Christov model for electrical magnetite micropolar Casson ferrofluid over a stretching/shrinking sheet using effective thermal conductivity model. *Case Stud. Therm. Eng.* **13**, 100352 (2019)
- Shahid, A.: The effectiveness of mass transfer in the MHD upper-convected Maxwell fluid flow on a stretched porous sheet near stagnation point: a numerical investigation. *Inventions* **5**(4), 64 (2020)
- Shahid, A., Huang, H., Bhatti, M.M., Zhang, L., Ellahi, R.: Numerical investigation on the swimming of gyrotactic microorganisms in nanofluids through porous medium over a stretched surface. *Mathematics* **8**(3), 380 (2020)
- Shahid, A., Huang, H., Khaliq, C., Bhatti, M.: Numerical analysis of activation energy on MHD nanofluid flow with exponential temperature-dependent viscosity past a porous plate. *J. Therm. Anal. Calorim.* **143**(3), 2585–2596 (2021)
- Sharanappa, D.S., Tawade, J.V., Veena, M., Pallavi, S.: MHD boundary layer flow of a Casson nano liquid over a penetrable linearly stretching sheet with frictional heating effects in Brinkmann–Forcheiemerr porous medium. *Mater. Today Proc.* (2020). <https://doi.org/10.1016/j.matpr.2020.10.125>
- Yahya, A.U., Salamat, N., Habib, D., Ali, B., Hussain, S., Abdal, S.: Implication of bio-convection and Cattaneo–Christov heat flux on Williamson Sutterby nanofluid transportation caused by a stretching surface with convective boundary. *Chin. J. Phys.* **73**, 706–718 (2021a)
- Yahya, A.U., Salamat, N., Huang, W.-H., Siddique, I., Abdal, S., Hussain, S.: Thermal characteristics for the flow of Williamson hybrid nanofluid ( $\text{MoS}_2 + \text{ZnO}$ ) based with engine oil over a stretched sheet. *Case Stud. Therm. Eng.* **26**, 101196 (2021b)